Rain statistics investigation and rain attenuation modeling for millimeter wave short-range fixed links

IEEE Access
Multidisciplinary | Rapid Review | Open Access Journal

Date of publication xxxx 00, 0000, date of current version xxxx 00, 0000.

Digital Object Identifier 10.1109/ACCESS.2019.DOI

Rain Statistics Investigation and Rain Attenuation Modeling for Millimeter Wave Short-range Fixed Links

JIE HUANG[1], YUSHENG CAO[1], XAVIER RAIMUNDO[1], ADNAN CHEEMA[2], AND SANA SALOUS[1], (Senior Member, IEEE)

[1]Department of Engineering, Durham University, Durham, DH1 3LE U.K.
[2]School of Engineering, Ulster University, Jordanstown Campus, Newtownabbey, BT370QB U.K.

Corresponding author: Sana Salous (e-mail: sana.salous@durham.ac.uk).

This work was supported in part by EPSRC under Grant EP/I00923X/1 "PARTICIAN: New Paradigms for Body Centric Wireless Communications at MM Wavelengths" and in part by Ofcom under Grant 1362 "Long term measurements campaign and development of model(s) for mm wave bands (30-90 GHz)".

ABSTRACT Millimeter wave (mmWave) communication is a key technology for fifth generation (5G) and beyond communication networks. However, the communication quality of the radio link can be largely affected by rain attenuation, which should be carefully taken into consideration when calculating the link budget. In this paper, we present results of weather data collected with a PWS100 disdrometer and mmWave channel measurements at 25.84 GHz (K band) and 77.52 GHz (E band) using a custom-designed channel sounder. The rain statistics, including rain intensity, rain events, and rain drop size distribution (DSD) are investigated for one year. The rain attenuation is predicted using the DSD model with Mie scattering and from the model in ITU-R P.838-3. The distance factor in ITU-R P.530-17 is found to be inappropriate for a short-range link. The wet antenna effect is investigated and additional protection of the antenna radomes is demonstrated to reduce the wet antenna effect on the measured attenuation.

INDEX TERMS 5G, ITU-R P.838-3 model, ITU-R P.530-17 model, millimeter wave, rain attenuation, disdrometer

I. INTRODUCTION

MILLIMETER wave (mmWave) communication is a key technology for fifth generation (5G) and beyond communication networks [1], [2]. It can be operated to provide high data rates in outdoor scenarios such as fronthaul, backhaul, and fixed link building to building transmission. However, the communication quality of the radio link can be largely affected by rain, fog, and vegetation attenuation, which should be carefully taken into consideration when calculating the link budget. Specifically, accurate modeling of snow and rain attenuation in the mmWave band is of utmost importance for 5G fixed link communication network deployment.

Rain will cause significant attenuation due to absorption and scattering for frequencies above 10 GHz. There have been several studies on the impact of rain attenuation on both satellite and terrestrial communication links. For satellite links, most of the beacon receivers are working at K-band (18-27 GHz). In [3], rain attenuation over a four year period was measured at Ka-band (19.7 and 20.2 GHz) based on the ONERA satellite link. The complementary cumulative distribution functions (CCDFs) of rain rate and rain attenuation were compared with ITU-R P.837-6 model. In [4], [5], rain and cloud attenuation was measured at 19.7 GHz and 39.4 GHz based on the Alphasat satellite links. In [6], rain attenuation was measured at Ka-band and Q-band (19.7 and 39.4 GHz) based on Eutelsat KA-SAT and Alphasat satellite, respectively. Both time diversity and orbital diversity were studied. In [7], rain attenuation was measured at 20.2 GHz based on Amazonas 3 satellite and compared with ITU-R P.618-13 model. In [8], rain attenuation was measured at 20.2 GHz and 30.5 GHz based on a GSAT-14 satellite in a tropical region. In [9], rain attenuation was measured based on a 19.7 GHz satellite link and a 38 GHz terrestrial link. The results for 75 GHz and 85 GHz terrestrial links are reported in [10].

Most of the reported measurements for terrestrial links, are for long-range ($>$ 1 km) links. For example, in [11], rain attenuation was measured at 38 GHz for a 1.85 km link. In

This article has been accepted for publication in a future issue of this journal, but has not been fully edited. Content may change prior to final publication. Citation information: DOI 10.1109/ACCESS.2019.2949437, IEEE Access

[12], rain attenuation was measured at a frequency range of 37.3-39.2 GHz for 8 links with distances between 48 m and 497 m. The results showed that wet antenna attenuation was 1.5-2, 2.8-5.3, and 6-9 dB for light rainfall rate (< 2 mm/h), heavy rainfall rate, and extreme rainfall rate (70-130 mm/h), respectively. In [13], rain attenuation was measured at 73 GHz for a 1 km link. The saturation value of wet antenna attenuation was suggested to be a random value. In [14], ten year rain attenuation was measured at 15, 21, and 38 GHz for a 1.1 km link. The rain drop size distribution (DSD) was fitted with a negative-exponential distribution. In [15], the rain attenuation was measured at 71-76 GHz for a 1 km link. The measured results were found to be in agreement with the ITU-R P.838-3 model. In [16], the results for a 60 GHz terrestrial link with distance of 150 m and K-band (12-18 and 28 GHz) satellite links were compared. The availability of the 60 GHz short-range link was almost constant over the observation time. In [17], rain attenuation was measured at 73, 83, 148, and 156 GHz over a distance of 325 m. Higher prediction accuracy was achieved using the DSD of rain. In [18], rain attenuation was measured at 26 GHz for a 1.3 km distance. The worst month statistic obtained from the real measurements was lower than what was predicted by the ITU-R P.581-2 model. In [19]–[21], rain attenuation was measured at 72 and 84 GHz. The results showed that the attenuation can be reduced by covering the antenna radome with additional hydrophobic material. The wet antenna effect on attenuation was found to have a maximum value of 2.3 dB.

In this paper, weather data using a PWS100 high-performance disdrometer and mmWave channel measurements at 25.84 GHz (K band) and 77.52 GHz (E band) are reported using a custom-designed channel sounder. The aim is to study the impact of precipitation on fixed links for short-range building to building transmission. The rain statistics, including rain intensity, rain events, and rain DSD are investigated for one year. The rain attenuation is predicted by the model in ITU-R P.838-3 and the DSD model with Mie scattering. The distance factor in ITU-R P.530-17 is applied. The wet antenna effect is investigated by comparing the measurement data before and after covering the antennas with additional protection to reduce the impact of the wetness of antenna radomes.

The rest of the paper is organized as follows. In Section II, the measurement setup of rain and rain attenuation is introduced. Section III shows the measurement results of rain statistics. The rain attenuation measurement results are shown in Section IV. In Section V, the rain attenuation prediction and wet antenna effect are investigated. Conclusions and future work are given in Section VI.

II. RAIN STATISTICS AND RAIN ATTENUATION MEASUREMENT SETUP

To study the impact of rain on fixed links, the custom-designed channel sounder reported in [22] is used. The sounder is upgraded with radio frequency (RF) heads at the 25.84 GHz and 77.52 GHz frequency bands, each with dual transmission and dual reception for polarization measurements [23]. The transmitter (Tx) and the receiver (Rx) reference generators up to the first intermediate frequency (IF) at 2.5 GHz and 2.501 GHz bands are placed in a room and are then fed via long cables to the second IF units; one at the transmitter and one at the receiver to generate signals at the second IF at about 12.92 GHz with a frequency difference of 2 MHz. The second IF signals are then in turn fed to the RF heads. The frequency offset of 1 MHz set up at the first IF leads to a down converted frequency of 4 MHz at the 25.84 GHz band and to 12 MHz at the 77.52 GHz band which allows combining the received signals from the two bands for each polarization into a single channel of the data acquisition card, which is controlled for simultaneous automatic recording of data from the four receivers. The channel data are recorded for one second every minute to relate with the rain rate data. The sampling rate of the RF link is 40 MHz and the attenuation per minute is an average over one second. The second IF and the RF heads and antennas are placed in weather proof boxes outside the building. The direct distance between the Tx antenna and Rx antenna is 35 m to investigate the impact of rain on typical building to building short-range links.

TABLE 1: Main parameters of the PWS100 present weather station.

Particle Size	0.1 to 30 mm
Size Accuracy	±5% (for particles larger than 0.3 mm)
Particle Velocity	0.16 to 30 m/s
Velocity Accuracy	±5% (for particles larger than 0.3 mm)
Types of Precipitation Detected	Drizzle, freezing drizzle, rain, freezing rain, snow grains, snowflakes, ice pellets, hail, graupel
Rain Rate Intensity Range	0 to 400 mm/h
Rainfall Resolution	0.0001 mm
Rain Total Accuracy	Typically ±10%

As shown in several studies, the wet antenna effect is an important factor that should be considered [13], [19], [24]. To investigate the wet antenna effect, measurements were conducted before and after covering the Tx and Rx antennas and their radomes with additional protective covers and a custom designed material that has lower retention of water than the standard radome. To relate the rain attenuation to actual rain events, a PWS100 high-performance disdrometer shown in Fig. 1(a) was installed with its readings recorded every minute. Table 1 lists its main specifications. The Tx antennas and Rx antennas with the additional coverage of radomes are shown in Fig. 1(b) and Fig. 1(c), respectively.

III. RAIN STATISTICS MEASUREMENT RESULTS

The weather station is located at (54.7679 N, 358.4267 W), and the data are collected from January 2018 to December 2018. The radio-meteorological data of one year have been submitted to the ITU study group 3 databanks (DBSG-3) [25], especially for Table IV-1 on statistics of rain intensity, Table IV-5 on statistics of rain event duration, and Table IV-

This article has been accepted for publication in a future issue of this journal, but has not been fully edited. Content may change prior to final publication. Citation information: DOI 10.1109/ACCESS.2019.2949437, IEEE Access

(a) PWS100 weather station (b) Transmit antennas (c) Receive antennas

FIGURE 1: Transmit and receive antennas with coverage of radomes.

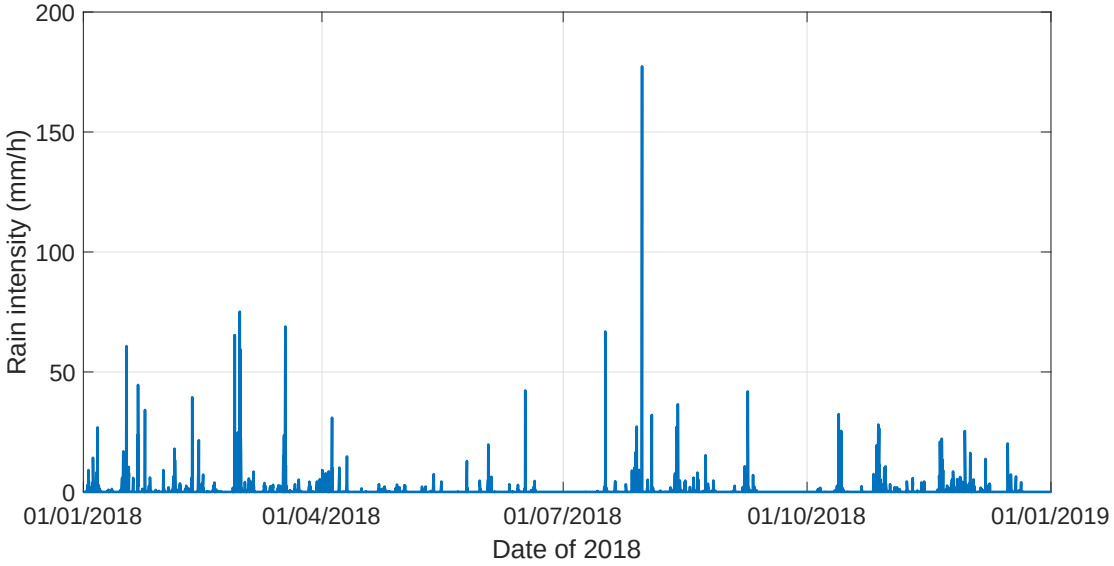

FIGURE 2: Rain intensity of each month.

12 on statistics of rain drop size distribution.

A. STATISTICS OF RAIN INTENSITY

Fig. 2 shows the rain intensity for each month. For most of the time, the maximum rain intensity is less than 70 mm/h. The worst month was July with a maximum rain intensity that exceeded 150 mm/h. Fig. 3 shows the CCDFs of the yearly rain intensity and worst month rain intensity that is exceeded for the given probability. The yearly rain intensity does not exceed 75.12 mm/h for a probability of 0.01%.

B. STATISTICS OF RAIN EVENT DURATION

Fig. 4 shows the total number of rain events and total rain event time. As the rain intensity increases, the total number of rain events and total rain event time tend to decrease. Fig. 5 shows the probability of occurrence (from 0 to 1) of rain events of duration longer than D (s), given that the rain rate is greater than R (mm/h). As the rain intensity and rain event duration time increases, the probability of occurrence of rain events decreases. Fig. 6 shows the total percentage of rain time (%) due to rain events of duration longer than D (s), given that the rain rate is greater than R (mm/h).

C. STATISTICS OF RAIN DSD

At high frequency bands, such as mmWave bands, rain attenuation is highly dependent on the DSD of rain. In weather data, 300 values of the number of particles with diameter range of 0.1-30 mm and particle size bin of 0.1 mm are recorded as well as the average velocity of all particles.

This article has been accepted for publication in a future issue of this journal, but has not been fully edited. Content may change prior to final publication. Citation information: DOI 10.1109/ACCESS.2019.2949437, IEEE Access

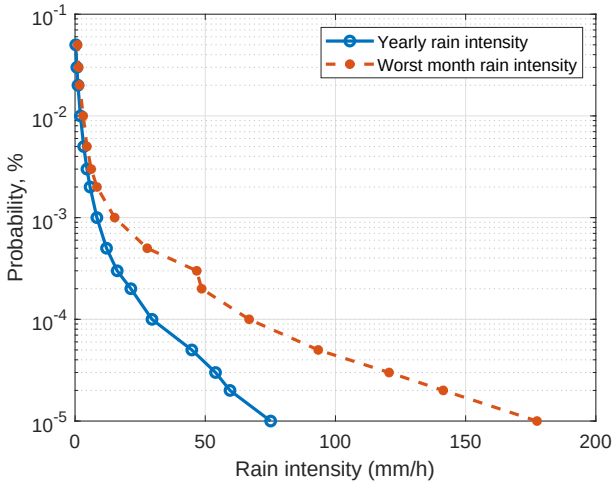

FIGURE 3: Yearly and worst month rain intensity CCDFs.

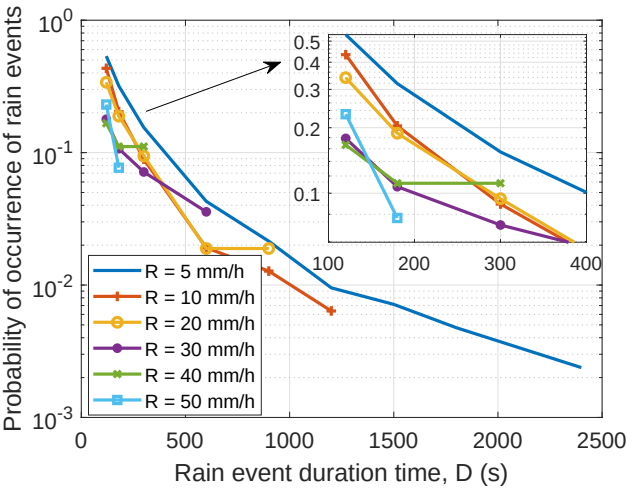

FIGURE 5: Probability of occurrence of rain events.

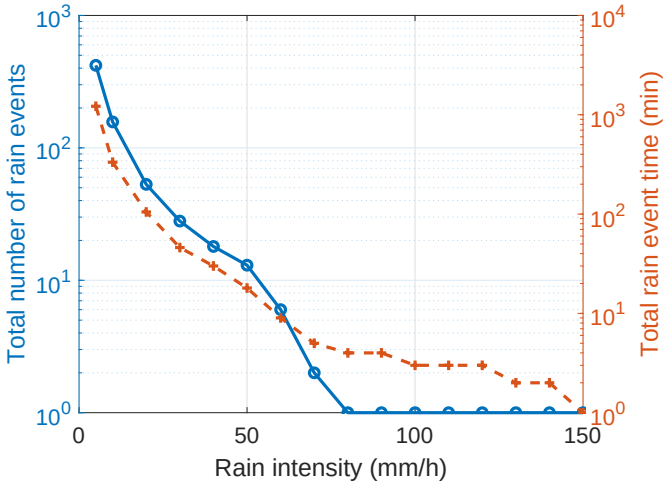

FIGURE 4: Total number of rain events and total rain event time.

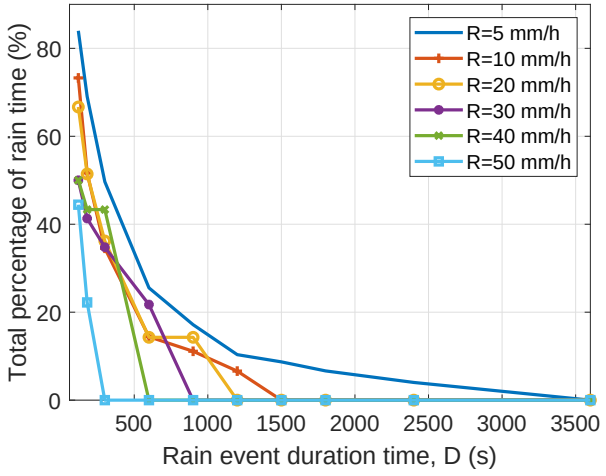

FIGURE 6: Total percentage of rain time.

The DSD can be calculated as:

$$N(D_i) = \sum_j \frac{n(D_i, v_j)}{v_j} \cdot \frac{1}{S \cdot \Delta t \cdot dD_i} \tag{1}$$

where $S = 40\ cm^2$ is the measurement surface of the laser beam of the PWS100 disdrometer, $\Delta t = 60$ s is the integration time, $n(D_i, v_j)$ is the number of particles registered within the classes with mean diameter D_i (mm) and mean speed v_j (m/s), dD_i (mm) is the class width associated with the diameter D_i. Rain rates less than 150 mm/h and rain drops with diameters less than 9.5 mm are classified as 43 and 23 bins to calculate the rain DSD values, respectively. Appropriate unit conversions are applied to obtian the result in $(m^{-3}mm^{-1})$.

As the velocity of each particle is not recorded, the theoretical relationship between the terminal fall velocity and the drop diameter is adopted for the computation of DSD. Specifically, the following equation is used:

$$v(D_i) = \begin{cases} 3.78 D_i^{0.67}, D_i < 0.8 \\ 9.65 - 10.3 e^{-0.6 D_i}, D_i \geq 0.8 \end{cases} \tag{2}$$

which is a combination of two widely used equations to achieve a non-negative and monotonic relation between the drop diameter and the terminal fall velocity [26], [27].

Three distribution models are applied to fit the rain DSD: the gamma distribution, the exponential distribution, and the lognormal distribution.

The gamma distribution model is given as:

$$N(D) = N_0 D^{\mu} \exp(-\lambda D) \tag{3}$$

where D (mm) is the rain drop diameter, N_0 is the intercept parameter, μ is the shape parameter, and λ is the slope parameter.

This article has been accepted for publication in a future issue of this journal, but has not been fully edited. Content may change prior to final publication. Citation information: DOI 10.1109/ACCESS.2019.2949437, IEEE Access

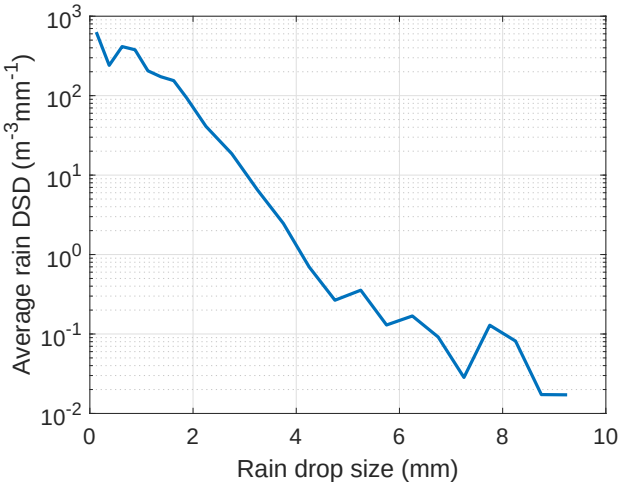

FIGURE 7: Average rain DSD over all rain bins.

TABLE 2: Fitting parameters of gamma distribution, exponential distribution, and lognormal distribution.

Rain rate (mm/h)	Gamma distribution (N_0, μ, λ)	Exponential distribution (N_0, λ)	Lognormal distribution (N_T, μ, σ)
1	(1423,1.0,3.337)	(257,1.643)	(125,-0.611,0.738)
2	(8970,2.3,3.896)	(328,0.939)	(288,-0.217,0.668)
3	$(1.68 \times 10^4$,2.8,4.220)	(366,0.831)	(264,-0.146,0.314)
5	$(1.24 \times 10^4$,2.5,3.704)	(434,0.776)	(334,-0.113,0.332)
10	(2830,1.2,2.064)	(576,0.740)	(480,-0.020,0.404)
20	(810,0.12,0.871)	(696,0.752)	(978,0.181,1.224)
40	(498,-0.3,0.459)	(737,0.753)	(1225,0.327,1.606)
60	(465,-0.93,0.230)	(2206,1.706)	(2358,-1,2.349)
70	(232,-2.19,-0.331)	(6000,2.177)	(2650,-1,0.855)

The exponential distribution model which is a special case of the gamma distribution with $\mu = 0$ is given as:

$$N(D) = N_0 \exp(-\lambda D) \tag{4}$$

The lognormal distribution model is expressed as:

$$N(D) = \frac{N_T}{\sigma D \sqrt{2\pi}} \exp\left(\frac{-(ln(D) - \mu)^2}{2\sigma^2}\right) \tag{5}$$

where N_T is the total number of drops, μ and σ are the mean and standard deviation of $ln(D)$, respectively.

Fig. 7 shows the average rain DSD over all rain bins. Fig. 8 shows the rain DSD and fitting results for rain bins with upper rain rates of 1, 2, 3, 5, 10, 20, 40, 60, and 70 mm/h. The fitting parameters of the gamma distribution, the exponential distribution, and the lognormal distribution are summarised in Table 2.

IV. RAIN ATTENUATION MEASUREMENT RESULTS

The set up was used to collect data from the disdrometer and from the dual-polarised dual-band fixed link measurements every minute. The PWS100 weather station data are logged in every minute and can be analysed to study the rain rate and the rain DSD. Previous studies have related these rain parameters to the effects of rain attenuation on radio links [28]–[30]. The collected fixed link data are analysed using the fast Fourier transform (FFT) and the signal peaks around the two frequencies of 4 MHz and 12 MHz are selected. The resulting received power is then classified as co-polarisation and cross-polarisation and these are mapped against the rain rate.

Fig. 9 and Fig. 10 show the measured fixed link data as well as rain and snow data in January 2018 for 25.84 GHz and 77.52 GHz, respectively. The slight fluctuations when there is no rain or snow is due to the limitation of power flatness of the measurement equipment and other small impacts such as temperature and humidity variations. The temperature and humidity relate to atmospheric attenuation, which is less than 0.5 dB for this short-range link. The received signal exhibited very slow variations, which were averaged out by a smoothing algorithm applied to the received signal over several minutes. The weather station is on the roof of a building and away from windbreaks. The antennas were covered only with radomes at the time of these measurements. The rain attenuation for 77.52 GHz is larger than that of 25.84 GHz. For 25.84 GHz, the cross-polarisation ratio (XPR) is about 15 dB, while it is about 20 dB for 77.52 GHz. The signal level follows the trend of rainfall rate. However, it can be observed that the signal level takes a long time to recover at the end of rain events, which can be more than two hours. Meanwhile, in some cases, the measured rain attenuation can be as high as 10 dB, which is much higher than the predicted rain attenuation by the ITU model in recommendation ITU-R P. 838-3 [31] for such a short link. The main cause for the signal level difference and signal level recovery time is the wet antenna effect. As the antenna is wet, rain drops attached to the antenna radome surface will cause additional attenuation. When the rain stops, it takes some time for the rain to evaporate. The heavy signal fading when there is no rain or with small rain rate is due to the attenuation caused by snow, which can be as much as 20 dB attenuation.

Fig. 11 shows a comparison of dry snow and wet snow attenuations for 77.52 GHz in February 2018. As can be seen, dry snow leads to small attenuation, while wet snow causes significant attenuation.

V. RAIN ATTENUATION PREDICTION AND WET ANTENNA EFFECT

A. RAIN ATTENUATION PREDICTION

Fig. 12 shows the measured co-polarisation attenuation at 77.52 GHz for three rain events. The maximum rain rate for the three rain events are 9 mm/h, 14 mm/h, and 34 mm/h, respectively. We then predict the rain attenuation using two models: the ITU-R P.838-3 model and the DSD model.

1) ITU-R P.838-3 Model and Distance Factor

The ITU-R P.838-3 model provides a relationship to predict rain attenuation. Though chosen for its simplicity, the empirical relationship given in (6) was validated both theoretically and experimentally:

$$\gamma = kR^{\alpha} \tag{6}$$

This article has been accepted for publication in a future issue of this journal, but has not been fully edited. Content may change prior to final publication. Citation information: DOI 10.1109/ACCESS.2019.2949437, IEEE Access

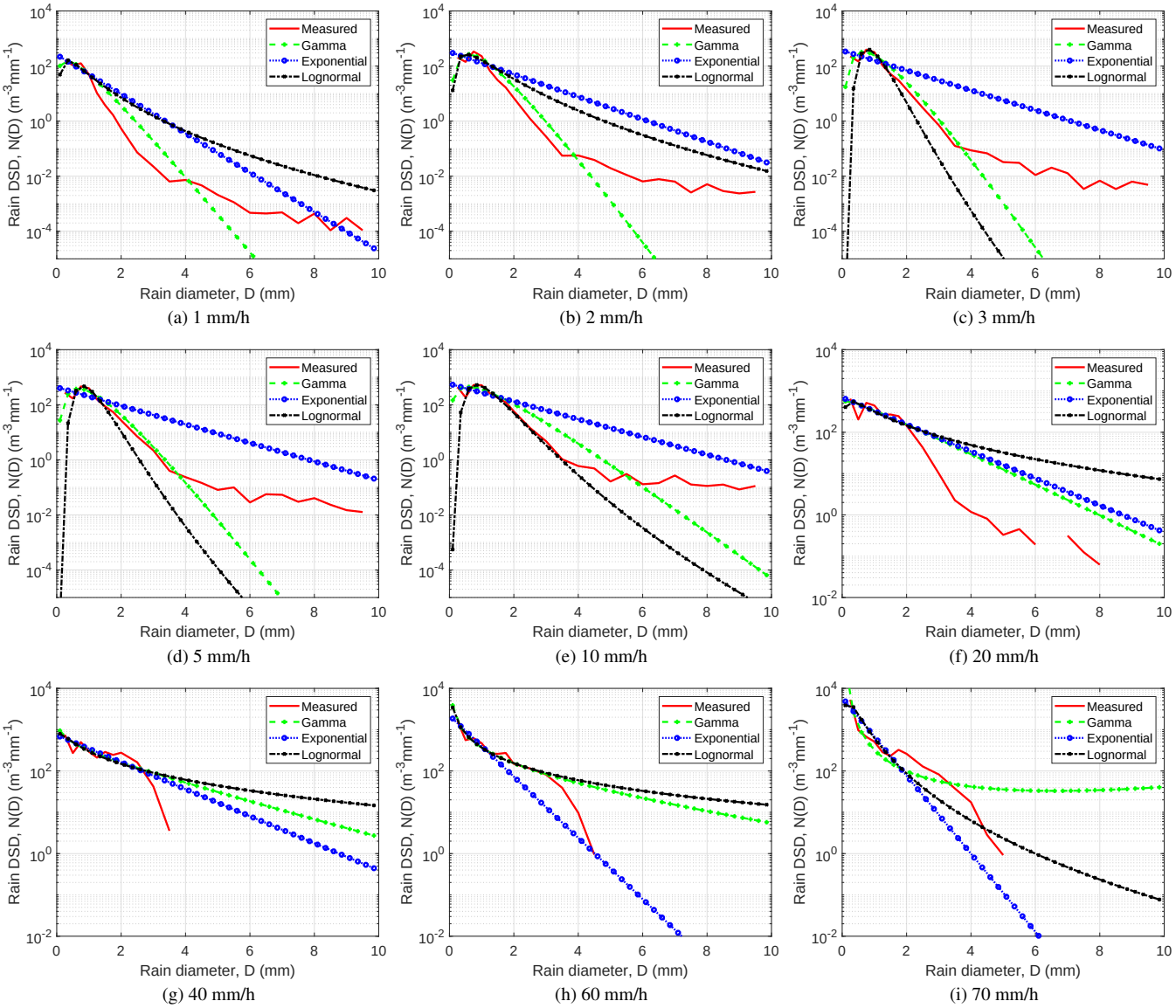

(a) 1 mm/h (b) 2 mm/h (c) 3 mm/h

(d) 5 mm/h (e) 10 mm/h (f) 20 mm/h

(g) 40 mm/h (h) 60 mm/h (i) 70 mm/h

FIGURE 8: Measured rain DSD and fitting results at different rain rates.

where R is the rain rate (mm/h), k and α are model parameters dependent on the frequency f, and γ is the specific attenuation in dB/km. For 77 GHz vertical polarisation, the specific coefficient values of k and α are 1.1276 and 0.7073, respectively.

The total attenuation for a specific distance depends on the effective path length d_{eff}, between the Tx and Rx antennas as:

$$A = \gamma d_{eff} \tag{7}$$

where the effective path length, d_{eff}, of the link is obtained by multiplying the actual path length d by a distance factor r.

In ITU-R P.530-17 [32] the distance factor is given as:

$$r = \frac{1}{0.477 d^{0.633} R_{0.01}^{0.073\alpha} f^{0.123} - 10.579(1 - exp(-0.024d))} \tag{8}$$

where $R_{0.01}$ is the rain rate exceeded for 0.01% of the time (with an integration time of 1 min). Note that (8) is first introduced in ITU-R P.530-14 and in force up to the latest ITU-R P.530-17 release, while the distance factor has a different expression in the previous releases. It is empirically derived with no direct link to the physics of radio wave propagation. The derivation is primarily based on long-range measurement datasets and 2.5 is given as the empirical maximum value. For the this study, d = 0.035 km, f = 77.52 GHz, α = 0.7073, and $R_{0.01}$ = 26.98 mm/h for January 2018, the calculated value of r is 9.37, which is much larger than the recommended maximum value of 2.5. For the 77.52 GHz band, the distance factor exceeds 2.5 when the distance is less than about 300 m under different $R_{0.01}$ values up to 160 mm/h. Later we will show that the maximum recommended distance factor is not appropriate for a short-range link.

This article has been accepted for publication in a future issue of this journal, but has not been fully edited. Content may change prior to final publication. Citation information: DOI 10.1109/ACCESS.2019.2949437, IEEE Access

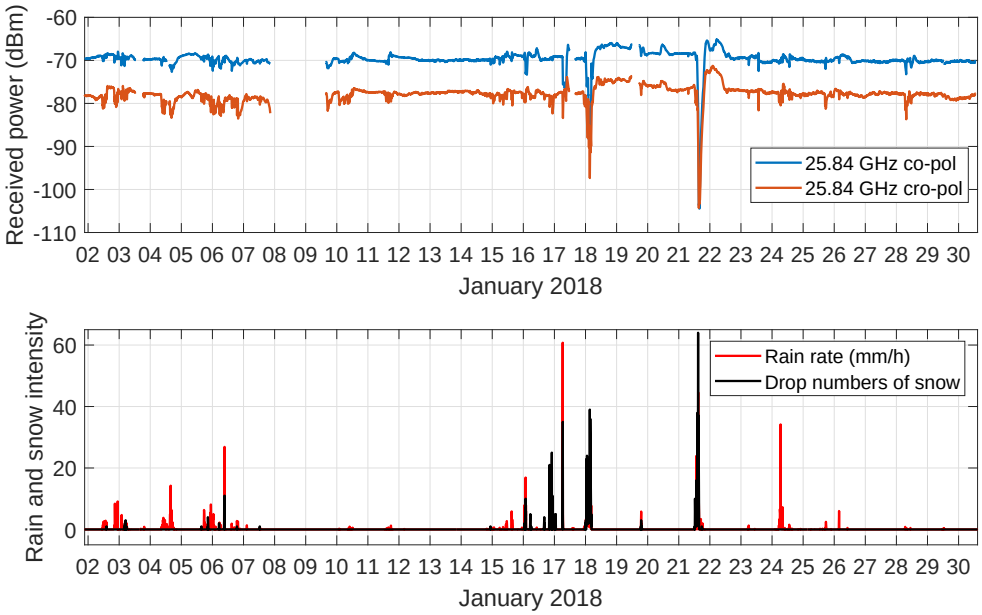

FIGURE 9: Measured fixed link data and rain data for 25.84 GHz in January 2018.

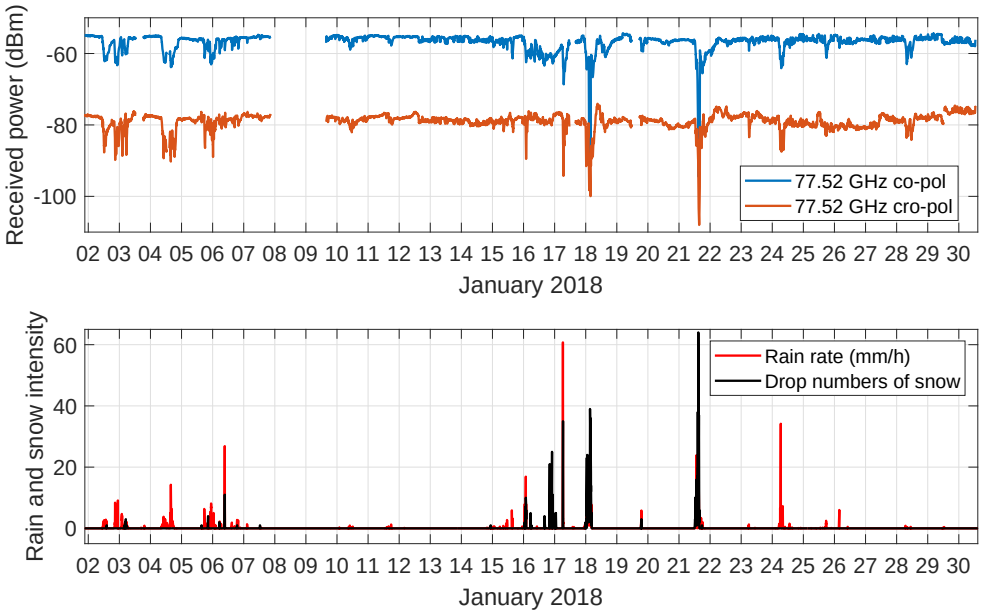

FIGURE 10: Measured fixed link data and rain data for 77.52 GHz in January 2018.

2) DSD Model and Rain Scattering Properties

The rain attenuation can be also predicted from the DSD model given by

$$\gamma = 4.343 \times 10^3 \int_0^\infty \delta_{ext}(D) N(D) dD \qquad (9)$$

where γ is the specific attenuation in dB/km, $\delta_{ext} = \pi(\frac{D}{2})^2 Q_{ext}$ is the extinction cross section (m^2) for water drops of diameter D (mm), and $N(D)$ is the drop size distribution value ($m^{-3}mm^{-1}$) at diameter D. The extinction efficiency Q_{ext} can be calculated from Mie scattering or Rayleigh scattering theory depending on the size parameter $x = \pi D/\lambda$, where λ is the wavelength.

For Rayleigh scattering, the extinction efficiency can be

This article has been accepted for publication in a future issue of this journal, but has not been fully edited. Content may change prior to final publication. Citation information: DOI 10.1109/ACCESS.2019.2949437, IEEE Access

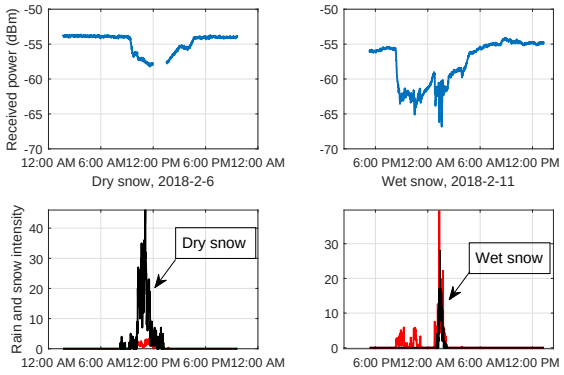

FIGURE 11: Comparison of dry snow and wet snow attenuations for 77.52 GHz in February 2018.

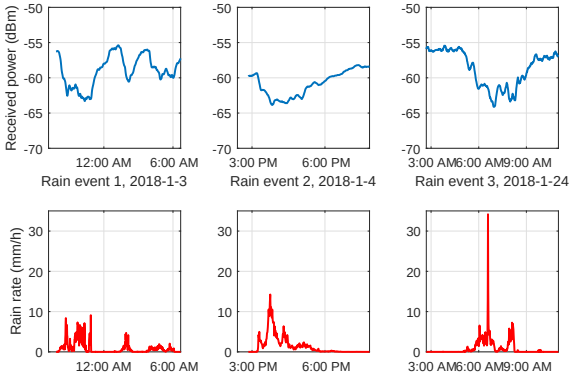

FIGURE 12: Measured co-polarisation attenuation for different rain and snow events at 77.52 GHz.

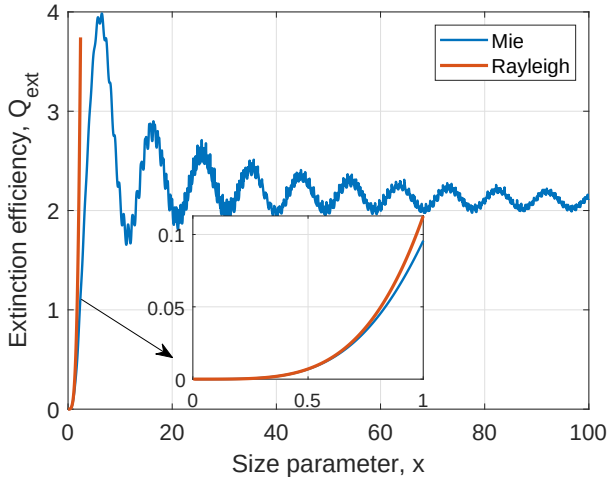

FIGURE 13: Extinction efficiency for Mie and Rayleigh scattering theory.

approximated as

$$Q_{ext} = 4x\text{Im}\left\{l(1+\frac{lx^2(m^4+27m^2+38)}{15(2m^2+3)})\right\}+\frac{8}{3}x^4\text{Re}\left\{l^2\right\} \quad (10)$$

TABLE 3: Percentage of Rayleigh scattering for 25.84 GHz and 77.52 GHz when $x < 0.6$

Percentage (%) of Rayleigh scattering ($x < 0.6$)	25.84 GHz	77.52 GHz
January	75.20	22.23
February	63.83	12.65
March	72.20	11.01
April	82.42	8.91
May	87.34	8.91
June	87.04	16.84
July	77.68	10.63
August	86.88	13.06
September	89.03	16.51
October	86.03	15.35
November	84.73	11.64
December	85.82	9.73
Total year	78.95	12.84

where $l = \frac{m^2-1}{m^2+2}$, m is the complex refractive index of the dielectric which has a value of 3.8528 + j2.0742 for water at 77.52 GHz, Re $\{\}$ and Im $\{\}$ are the real part and imaginary part, respectively.

For Mie scattering, the extinction efficiency is calculated as:

$$Q_{ext} = \frac{2}{x^2}\sum_{n=1}^{\infty}(2n+1)\text{Re}\left\{a_n+b_n\right\} \quad (11)$$

$$a_n = \frac{\psi_n'(mx)\psi_n(x) - m\psi_n(mx)\psi_n'(x)}{\psi_n'(mx)\xi_n(x) - m\psi_n(mx)\xi_n'(x)} \quad (12)$$

$$b_n = \frac{m\psi_n'(mx)\psi_n(x) - \psi_n(mx)\psi_n'(x)}{m\psi_n'(mx)\xi_n(x) - \psi_n(mx)\xi_n'(x)} \quad (13)$$

where $\psi_n(x)$ and $\xi_n(x)$ are the Riccati-Bessel functions and can be expressed using spherical Bessel functions of the first kind and third kind as:

$$\psi_n(x) = \sqrt{\frac{\pi x}{2}}J_{n+\frac{1}{2}}(x) \quad (14)$$

$$\xi_n(x) = \sqrt{\frac{\pi x}{2}}H^{(2)}_{n+\frac{1}{2}}(x). \quad (15)$$

Rayleigh scattering occurs when $x \ll 1$, while Mie scattering is not restricted by the size parameter. When $x < 0.6$, the extinction efficiency for Mie and Rayleigh scattering is close, as shown in Fig. 13. Table 3 gives the percentage of Rayleigh scattering for 25.84 GHz and 77.52 GHz when $x < 0.6$. On average, 78.95% and 12.84% of the scattering can be attributed to Rayleigh scattering for 25.84 GHz and 77.52 GHz, respectively. For the 77.52 GHz band, the Mie scattering assumption is more realistic.

Fig. 14 shows the predicted rain attenuation in dB/km using (6) and (9) for the three rain events applying the ITU-R P. 838-3 model and the DSD model with Mie scattering, respectively. For lower rain rates, the ITU model predicted attenuation is slightly larger than the DSD model, while for higher rain rates, the ITU model predicted attenuation is smaller than the DSD model.

Fig. 15 shows the measured and predicted rain attenuations for 77.52 GHz without using the recommended maximum

This article has been accepted for publication in a future issue of this journal, but has not been fully edited. Content may change prior to final publication. Citation information: DOI 10.1109/ACCESS.2019.2949437, IEEE Access

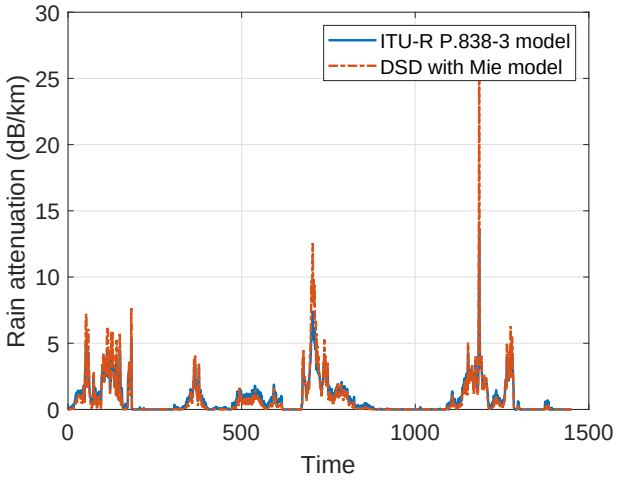

FIGURE 14: Predicted rain attenuation at 77.52 GHz using ITU model and DSD model.

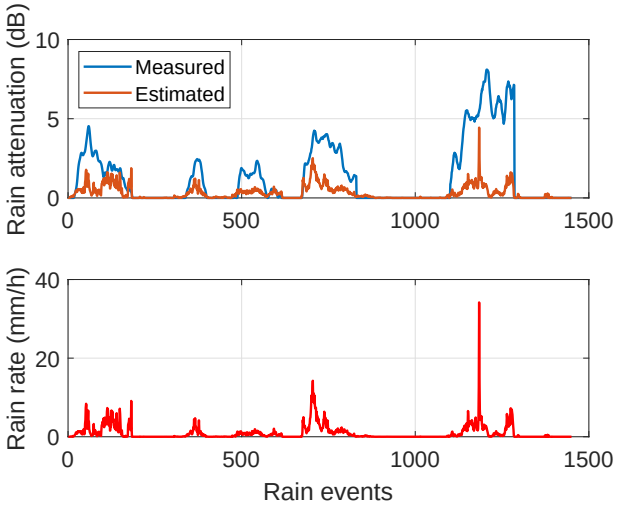

FIGURE 15: Measured and predicted 77.52 GHz rain attenuations without using the maximum distance factor of 2.5.

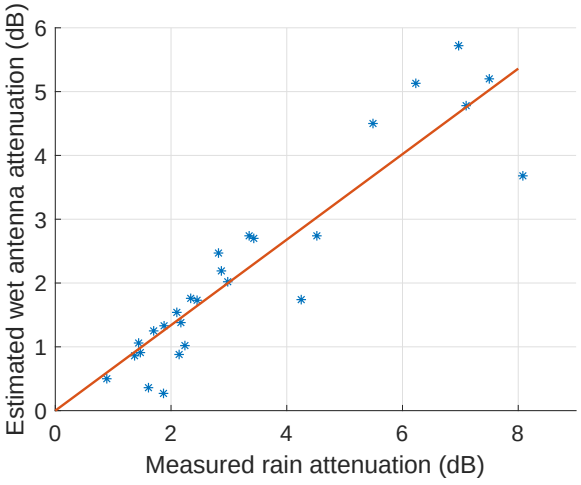

FIGURE 16: Relationship between measured total rain attenuation and the estimated wet antenna attenuation.

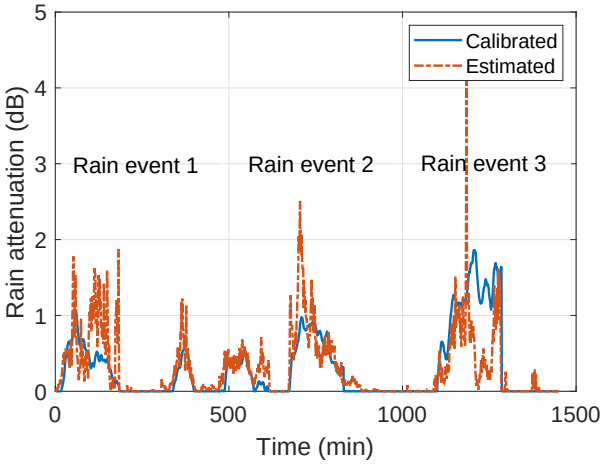

FIGURE 17: Comparison between predicted attenuation with ITU model and the corrected measured attenuation.

distance factor of 2.5. The difference between the measured and estimated attenuation has been significantly reduced with the remaining difference between the measured and predicted attenuations being due to the wet antenna effect. If the distance factor is set at 2.5, the difference between the measured and estimated attenuations will be even larger.

B. WET ANTENNA EFFECT

In [24] the wet antenna effect is modelled by an exponential distribution. To identify a suitable model from the current measurements we extract the total attenuation from the measurement data as A_m and use the ITU model to predict the rain attenuation A_i. This gives the attenuation caused by the wet antenna as:

$$A_w = A_m - A_i. \tag{16}$$

To find the relationship between the measured attenuation and the wet antenna attenuation, we select several peak rain rates and the measured attenuations, as shown in Fig. 16. A simple linear fit with a coefficient of 0.67 is found to be reliable, i.e., $A_i = 0.33A_m$. This indicates that the additional attenuation caused by the wet antennas accounts for 67% of the total attenuation for a short link.

Fig. 17 shows the predicted attenuation by the ITU model without the maximum distance restriction of 2.5 in the recommendation and the calibrated attenuation after removing the wet antenna effect by applying the linear fit model. A good agreement can be achieved for most of the attenuations, except for some high peak rain rates.

As a comparison, Fig. 18 shows the measured 77.52 GHz rain attenuation in January 2018 to be about 8 dB at 9 mm/h rain fall rate while it is about 8 dB at 16 mm/h rain rate for the 30th of November 2018 after the additional coverage of

This article has been accepted for publication in a future issue of this journal, but has not been fully edited. Content may change prior to final publication. Citation information: DOI 10.1109/ACCESS.2019.2949437, IEEE Access

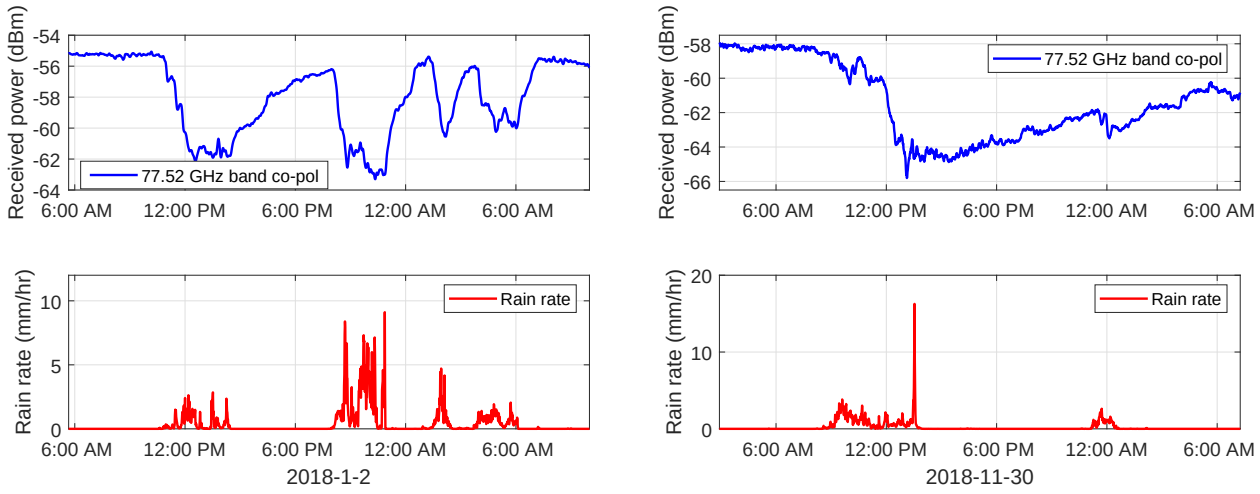

(a) Before the coverage of antennas

(b) After the coverage of antennas

FIGURE 18: Measured 77.52 GHz rain attenuation: (a) Before the coverage of antennas and (b) After the coverage of antennas.

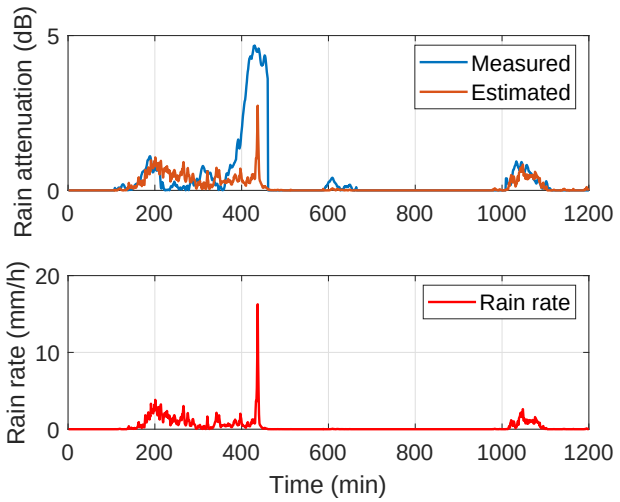

FIGURE 19: Measured and predicted 77.52 GHz rain attenuation after the coverage of antennas.

the antennas. This indicates a reduction in the wet antenna effect on the measured attenuation.

Fig. 19 shows the measured and predicted attenuations. For similar rain fall rates, the difference between the measured and predicted results are now within 2 dB, in comparison to 5 dB prior to the additional coverage of antennas; giving a 3 dB reduction of the wet antenna effect. When the rain rate is smaller than 5 mm/hr, the wetness of the antennas is very small, and the predicted and the measured attenuation are similar. However, for higher rain rates such as 16 mm/h, the wet antenna effect has a comparable attenuation to the rain attenuation and cannot be ignored.

VI. CONCLUSIONS AND FUTURE WORK

A custom-designed channel sounder was with dual-polarized transmitters and receivers have been set up over a short link typical of a building to building scenario to study the impact of rain on the 25.84 GHz and 77.52 GHz bands identified for future 5G and beyond communication systems. A high-performance disdrometer was used to collect weather data. The ITU-R P.838-3 rain attenuation model and the DSD model are compared, and the maximum recommended distance factor in ITU-R P.530-17 is shown to be inappropriate for a short-range link. The wet antenna effect is investigated, and the attenuation can be further reduced by 2-3 dB, which is about 50% of the attenuation caused by wet antennas with additional coverage. A simple linear fit model for measured attenuation can be also applied to reduce the antenna wetness effect and gives results comparable to the ITU model without using the maximum distance factor.

Further work is currently being undertaken to upgrade the set up with a phase locked loop (PLL) to generate the second IF directly at 12.92 GHz. This enables the IF generator to be housed with the RF heads; thus reducing the complexity and the impact of rain on the interconnection between units and the need for RF cables. Apart from the cables from the rubidium standard reference clock to the PLL and the data acquisition cards, and the cables from the receivers outputs, all units at each end of the link will be housed within a single weather proof box. In addition, another link using Filtronic RF heads to extend the measurement distance, and a third receiver are added to the short link to capture scattered energy. Work is also being undertaken to improve the system performance, and collect more measurement data to generate interference models and rain statistics for 5G long term fixed links.

ACKNOWLEDGMENT

The authors would like to thank the late Stuart Feeney for the realisation of the sounder, Ian Hutchinson, Neil Clarey, and Colin Dart from the electronic workshop and Colin Wintrip from the mechanical workshop at Durham University for the set up of the link.

REFERENCES

[1] S. Salous et al., "Millimeter-wave propagation: Characterization and modeling toward fifth-generation systems," IEEE Antennas Propag. Mag., vol. 58, no. 6, pp. 115–127, Dec. 2016.

[2] J. Huang, C.-X. Wang, R. Feng, J. Sun, W. Zhang, and Y. Yang, "Multi-frequency mmWave massive MIMO channel measurements and characterization for 5G wireless communication systems," IEEE J. Sel. Areas Commun., vol. 35, no. 7, pp. 1591–1605, July 2017.

[3] X. Boulanger, B. Gabard, L. Casadebaig, and L. Castanet, "Four years of total attenuation statistics of earth-space propagation experiments at Ka-band in Toulouse," IEEE Trans. Antennas Propag., vol. 63, no. 5, pp. 2203–2214, May 2015.

[4] L. Luini, C. G. Riva, L. Emiliani, and J. Nessel, "Modeling the impact of rain and clouds on earth–space site diversity systems," IEEE Trans. Antennas Propag., vol. 67, no. 1, pp. 475–483, Jan. 2019.

[5] L. Quibus, L. Luini, C. Riva, and D. Vanhoenacker-Janvier, "Use and accuracy of numerical weather predictions to support EM wave propagation experiments," IEEE Trans. Antennas Propag., 2019, in press.

[6] D. Pimienta-Del-Valle, J. M. Riera, and P. Garcia-Del-Pino, "Time and orbital diversity assessment with Ka- and Q-band slant-path propagation experiments in Madrid," IEEE Trans. Antennas Propag., vol. 67, no. 2, pp. 1193–1201, Feb. 2019.

[7] X. Boulanger, B. Benammar, and L. Castanet, "Propagation experiment at Ka-band in French Guiana: First year of measurements," IEEE Antennas Wireless Propag. Lett., vol. 18, no. 2, pp. 241–244, Feb. 2019.

[8] M. K. Mishra, R. Renju, N. Mathew, C. Suresh Raju, M. Sujimol, and K. Shahana, "Rain attenuation of Ka-band signal over a Tropical station," in Proc. 2019 URSI Asia-Pacific Radio Science Conference (AP-RASC), New Delhi, India, 2019, pp. 1–3.

[9] J. M. García-Rubia, J. M. Riera, A. Benarroch, and P. Garcia-del-Pino, "Estimation of Rain attenuation from experimental drop size distributions," IEEE Antennas Wireless Propag. Lett., vol. 10, pp. 839–842, 2011.

[10] J. M. García-Rubia, J. M. Riera, P. Garcia-del-Pino, and A. Benarroch, "Attenuation measurements and propagation modeling in the W-band," IEEE Trans. Antennas Propag., vol. 61, no. 4, pp. 1860–1867, Apr. 2013.

[11] M. Schleiss, J. Rieckermann, and A. Berne, "Quantification and modeling of wet-antenna attenuation for commercial microwave links," IEEE Geosci. Remote Sens. Lett., vol. 10, no. 5, pp. 1195–1199, Sept. 2013.

[12] M. Fencl, P. Valtr, M. Kvičera, and V. Bareš, "Quantifying wet antenna attenuation in 38-GHz commercial microwave links of cellular backhaul," IEEE Geosci. Remote Sens. Lett., vol. 16, no. 4, pp. 514–518, Apr. 2019.

[13] J. Ostrometzky, R. Raich, L. Bao, J. Hansryd, and H. Messer, "The wet-antenna effect — A factor to be considered in future communication networks," IEEE Trans. Antennas Propag., vol. 66, no. 1, pp. 315–322, Jan. 2018.

[14] T.-S. Yeo, P.-S. Kooi, M.-S. Leong, and L.-W. Li, "Tropical raindrop size distribution for the prediction of rain attenuation of microwaves in the 10-40 GHz band," IEEE Trans. Antennas Propag., vol. 49, no. 1, pp. 80–83, Jan. 2001.

[15] J. Hansryd, Y. Li, J. Chen, and P. Ligander, "Long term path attenuation measurement of the 71–76 GHz band in a 70/80 GHz microwave link," in Proc. EuCAP'10, Barcelona, 2010, pp. 1-4.

[16] W. Chujo, T. Manabe, and S. Yamamoto, "60-GHz short-range terrestrial rainfall attenuation compared with K-band long-distance satellite link," in Proc. 2014 International Symposium on Antennas and Propagation Conference Proceedings, Kaohsiung, 2014, pp. 559–560.

[17] L. Luini, G. Roveda, M. Zaffaroni, M. Costa, and C. Riva, "EM wave propagation experiment at E band and D band for 5G wireless systems: Preliminary results," in Proc. EuCAP'18, London, 2018, pp. 1–5.

[18] I. Shayea, T. Abd. Rahman, M. Hadri Azmi, and M. R. Islam, "Real measurement study for rain rate and rain attenuation conducted over 26 GHz microwave 5G link system in Malaysia," IEEE Access, vol. 6, pp. 19044–19064, 2018.

[19] E. S. Hong, S. Lane, D. Murrell, N. Tarasenko, and C. Christodoulou, "Mitigation of reflector dish wet antenna effect at 72 and 84 GHz," IEEE Antennas Wireless Propag. Lett., vol. 16, pp. 3100–3103, 2017.

[20] E. S. Hong, S. Lane, D. Murrell, N. Tarasenko, and C. Christodoulou, "Terrestrial link rain attenuation measurements at 84 GHz," in Proc. 2017 United States National Committee of URSI National Radio Science Meeting (USNC-URSI NRSM), Boulder, CO, 2017, pp. 1–2.

[21] E. S. Hong, S. Lane, D. Murrell, N. Tarasenko, C. Christodoulou, and J. Keeley, "Estimating rain attenuation at 72 and 84 GHz from raindrop size distribution measurements in Albuquerque, NM, USA," IEEE Geosci. Remote Sens. Lett., 2019, in press.

[22] S. Salous, S. M. Feeney, X. Raimundo, and A. A. Cheema, "Wideband MIMO channel sounder for radio measurements in the 60 GHz band," IEEE Trans. Wireless Commun., vol. 15, no. 4, pp. 2825–2832, Apr. 2016.

[23] S. Salous, Y. Cao, and X. Raimundo, "Impact of precipitation on millimetre wave fixed links," in Proc. EuCAP'19, Krakow, Poland, Apr. 2019.

[24] M. M. Z. Kharadly and R. Ross, "Effect of wet antenna attenuation on propagation data statistics," IEEE Trans. Antennas Propag., vol. 49, no. 8, pp. 1183–1191, Aug. 2001.

[25] ITU-R website, https://www.itu.int/en/ITU-R/study-groups/rsg3/Pages/dtbank-dbsg3.aspx

[26] D. Atlas and C.W. Ulbrich, "Path- and area-integrated rainfall measurement by microwave attenuation in the 1-3 cm band," J. Appl. Meteorol., vol. 16, pp. 1322–1331, 1977.

[27] D. Atlas, R.C. Srivastava, and R.S. Sekhon, "Doppler radar characteristics of precipitation at vertical incidence," Rev. Geophys., vol. 11, pp. 1–35, 1973.

[28] J. Marshall and W. Palmer, "The distribution of raindrops with size," Journal of Meteorology, vol. 5, no. 4, pp. 165–166, 1948.

[29] C. Ulbrich, "Natural variations in the analytical form of the raindrop size distribution," Journal of Climate and Applied Meteorology, vol. 22, no. 10, pp. 1764–1775, 1983.

[30] C. You, D. Lee, M. Kang, and H. Kim, "Classification of rain types using drop size distributions and polarimetric radar: Case study of a 2014 flooding event in Korea," Atmospheric Research, vol. 181, pp. 211–219, 2016.

[31] ITU-R P. 838-3, Specific attenuation model for rain for use in prediction methods.

[32] ITU-R P. 530-17, Propagation data and prediction methods required for the design of terrestrial line-of-sight systems.

JIE HUANG received the B.E. degree in Information Engineering from Xidian University, China, in 2013, and the Ph.D. degree in Communication and Information Systems from Shandong University, China, in 2018. He received the Best Student Paper Award at WPMC'16. He joined the Mobile Communications Research Laboratory, Southeast University, China, in Oct. 2018. He is currently a Postdoctoral Research Associate in Durham University, U.K. His research interests include millimeter wave and massive MIMO channel measurements, parameter estimation, channel modeling, wireless big data, rain attenuation, and 5G/B5G wireless communications.

YUSHENG CAO received the B.E. degree from Harbin Institute of Technology, China, in 2012, and the M.Sc. degree from The University of Sheffield, U.K., in 2014. He is currently a PhD student at Durham University, U.K. His research interests include mmWave channel measurements and rain attenuation prediction.

XAVIER RAIMUNDO received his B.E. degree and M.Sc. degree from Kings College London in 2008 and 2009, respectively. He subsequently joined Durham University as a PhD student working on radar imaging. Following the award of his PhD he joined Durham University as a Postdoctoral Research Associate working on radio 5G radio propagation measurements and modeling.

ADNAN CHEEMA received his B.Sc. degree in Computer Engineering from COMSATS University, Pakistan and M.Sc. degree in Signal Processing for Communication from Kings College London, U.K. He then joined Durham University, U.K. for his Ph.D. studies working on cognitive radio and spectrum sensing. In 2015, he took up a Postdoctoral Research Associate position at Durham University, U.K. working on 5G radio propagation measurements and modeling (sub-6 GHz and 24-90 GHz). In 2017, he joined Ulster University, U.K., as a lecturer in Electronics Engineering.

SANA SALOUS (SM'95) received the B.E.E. degree from the American University of Beirut, Beirut, Lebanon, in 1978, and the M.Sc. and Ph.D. degrees from Birmingham University, Birmingham, U.K., in 1979 and 1984, respectively.

She was an Assistant Professor with Yarmouk University, Irbid, Jordan, for four years followed by one year Research Fellowship at Liverpool University, Liverpool, U.K. She held a lectureship with the University of Manchester Institute of Science and Technology, Manchester, U.K., in 1989, where she was subsequently a Senior Lecturer and then a Reader. Since 2003, she has held the Chair in Communications Engineering at Durham University, Durham, U.K., where she is currently the Director of the Centre for Communication Systems. Her current research interests include radio channel characterization in various frequency bands ranging from skywave in the HF band to millimeter wave bands, the design of radar waveforms, and novel radio channel sounders and radar systems for radio imaging.

Dr. Salous is a Fellow of the Institution of Engineering and Technology (FIET) and a Fellow of the International Union of Radio Science (FURSI). She was the Chair of Commission C on Radio Communication and Signal Processing Systems of URSI (2014-2017). She is the Editor in Chief of the journal Radio Science, a publication of the American Geophysical Union.